From antiferromagnetism to superconductivity in $Fe_{1+y}Te_{1-x}Se_x$ ($0 \leq x \leq 0.20$): Neutron powder diffraction analysis

A. Martinelli,[1,*] A. Palenzona,[1,2] M. Tropeano,[1,3] C. Ferdeghini,[1] M. Putti,[1,3] M. R. Cimberle,[4] T. D. Nguyen,[5] M. Affronte,[5] and C. Ritter[6]

[1]*CNR-SPIN, Corso Perrone 24, 16152 Genova, Italy*

[2]*Dipartimento di Chimica e Chimica Industriale, Università di Genova, via Dodecaneso 31, 16146 Genova, Italy*

[3]*Dipartimento di Fisica, Università di Genova, via Dodecaneso 33, 16146 Genova, Italy*

[4]*Dipartimento di Fisica, CNR-IMEM, via Dodecaneso 33, 16146 Genova, Italy*

[5]*CNR Institute of Nanosciences S3 and Dipartimento di Fisica, Università di Modena e Reggio Emilia, via G. Campi 213A, 41125 Modena, Italy*

[6]*Institute Laue-Langevin, 6 rue Jules Horowitz, 38042 Grenoble Cedex 9, France*

The nuclear and magnetic structures of $Fe_{1+y}Te_{1-x}Se_x$ ($0 \leq x \leq 0.20$) compounds was analyzed between 2 and 300 K by means of Rietveld refinement of neutron powder diffraction data. Samples with $x \leq 0.075$ undergo a tetragonal to monoclinic phase transition at low temperature, whose critical temperature decreases with increasing Se content; this structural transition is strictly coupled to a long-range antiferromagnetic ordering at the Fe site. Both the transition to a monoclinic phase and the long-range antiferromagnetism are suppressed for $0.10 \leq x \leq 0.20$. The onset of the structural and of the magnetic transition remains coincident with the increase in Se substitution. The low-temperature monoclinic crystal structure has been revised. Superconductivity arises for $x \geq 0.05$, therefore a significant region where superconductivity and long-range antiferromagnetism coexist is present in the pseudobinary FeTe-FeSe phase diagram.

I. INTRODUCTION

The end members of the solid solution $Fe_{1+y}Te_{1-x}Se_x$ belong to the class of compounds characterized by the presence of edge-sharing Fe-centered tetrahedra, forming layered structures that attracted much attention on account of the discovery of a relatively high superconducting transition temperature (T_c) in $LaFeAs(O_{1-x}F_x)$.[1] Both FeTe and FeSe are isostructural with α-PbO, crystallizing at room temperature in the tetragonal system ($P4/nmm$ space group) and they are both referred to as β phase.[2,3] It is worth pointing out that $Fe_{1+y}Te_{1-x}Se_x$ compounds are often referred to as α phase in the literature, probably because they are isostructural with α-PbO. However, in the Fe-Te and Fe-Se phase diagrams the notation α refers only to the terminal Fe-rich solid solutions or to the low-temperature monoclinic phase α-Fe_7Se_8.

Subtle stoichiometric variations in $Fe_{1+y}Se$ can determine different structural and resistive properties: for $y=0.01$ the phase can exhibit a structural transition on cooling followed by the rise of superconductivity, whereas for $y=0.03$ the structural change is suppressed as well as the superconductive transition.[4] The structural properties of $Fe_{1+y}Te$ are as well strongly affected by faint stoichiometrical variations: compounds with $y=0.141$ and 0.076 crystallize at low temperature in the orthorhombic ($Cmme$ space group) and monoclinic ($P2/_1m$ space group) system, respectively.[5] Antiferromagnetic (AFM) spin ordering occurs in these $Fe_{1+y}Te$ compounds at the Fe site at low temperature, characterized by a commensurate magnetic wave vector $\mathbf{q}=(\frac{1}{2}\ 0\ \frac{1}{2})$ when it is associated to the monoclinic structure and incommensurate in the orthorhombic one.[5] Partial substitution of Te with Se progressively suppresses the tetragonal to monoclinic

phase transition and induces superconductivity at low temperature. Static long-range (LR) magnetic order is suppressed as well on Se doping, although short range (SR) not commensurate AFM fluctuations are still present in samples with $x=0.25$ exhibiting a trace of superconductivity,[6] as well as in superconducting samples with x ranging from 0.30 to 0.416.[5,7] Coexistence between incommensurate SR-AFM and superconductivity has been also reported by Khasanov *et al.*[8] in samples with $0.25 \leq x \leq 0.40$, whereas commensurate magnetic order prevails for $x \leq 0.10$.

At present it is not yet clear whether the tetragonal to monoclinic transition occurring in FeTe on cooling is driven by magnetism or not; Li *et al.*[7] argue from specific-heat measurements that this structural transition is driven by magnetism. Conversely McQueen *et al.*[4] analyzed the tetragonal to orthorhombic transition taking place in FeSe. As there is no magnetic order present even at low temperature in this compound they concluded that magnetism is not the driving force for the structural transition even in the other superconducting pnictides. By means of neutron powder diffraction (NPD) we analyze in this paper the evolution from the AFM ground state of FeTe to the superconducting one and the suppression of the structural and magnetic transition by substituting Te with Se up to $x=0.20$.

II. EXPERIMENTAL

Samples of $Fe_{1+y}Te_{1-x}Se_x$ with $x=0.00, 0.025, 0.05, 0.075, 0.10, 0.15, 0.20$ were prepared by means of a solid-state reaction in two steps: (1) a mixture of stoichiometric amounts of pure elements was reacted in a sealed evacuated Pyrex tube at 400–450 °C for 15–20 h and (2) the so-obtained product was ground, pelletized, and heated at
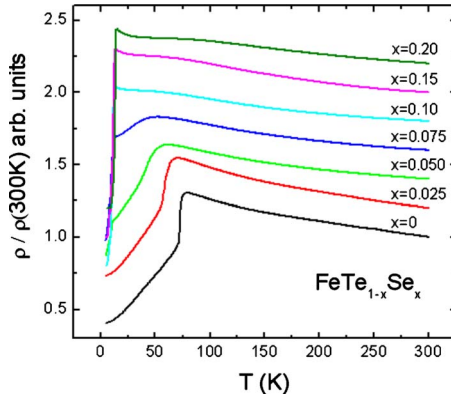
FIG. 1. (Color online) Resistivities for FeTe$_{1-x}$Se$_x$ samples normalized to room temperature.

800 °C for 7–8 days in a sealed evacuated quartz tube. All the operations were carried out in a glove box with O_2 and H_2O partial pressures less than 1 ppm.

NPD experiments were carried out at the Institute Laue Langevin (Grenoble—France). In order to evaluate the temperature at which the structural and magnetic transitions take place, thermodiffractograms of the samples with x =0.00, 0.025, 0.05, 0.075 were acquired on heating in continuous scanning mode in the T range 1.5–80 K using the high intensity D1B diffractometer (λ=2.52 Å). High-resolution NPD patterns were collected at selected temperatures between 2 and 300 K using the D1A diffractometer (λ=1.91 Å) for the samples with x =0.00, 0.05, 0.10, 0.15, 0.20. Rietveld refinement of NPD data was carried out using the program FULLPROF;[9] by means of a NAC standard an instrumental resolution file was obtained and applied during refinements in order to detect microstructural contributions to the NPD peak shape. The diffraction lines were modeled by a Thompson-Cox-Hastings pseudo-Voigt peak shape function convoluted with an axial divergence asymmetry function. The background was fitted by a fifth-order polynomial. The following parameters were refined in the last cycle of calculation: the overall scale factor; the background (five parameters of the fifth-order polynomial); 2θ-zero; the unit-cell parameters; the specimen displacement; the reflection-profile asymmetry; the Wyckoff positions not constrained by symmetry; the isotropic thermal parameters B; the anisotropic strain parameters; and the occupancy (y) at the interstitial Fe site.

Resistive measurements were carried out in a physical properties measurements system (PPMS, Quantum Design) in the temperature range 5–300 K. Heat capacity was measured on pellets by a Quantum Design PPMS. The heat pulse was fixed in order to have 1% in temperature response and the two-tau relaxation method was necessary to account for the low thermal conductivity of the samples.

III. RESULTS AND DISCUSSION

A. Resistivity

Resistivity measurements of Fe$_{1+y}$Te$_{1-x}$Se$_x$ samples are shown in Fig. 1. With decreasing temperature the resistivity

TABLE I. Critical temperatures for the tetragonal to monoclinic structural change, the long-range AFM ordering, and the superconductive transition.

Se content(x)	$T_{\text{T-M}}$ (K)	T_{N} (K)	T_{c} (K)
0.00	72.5 ± 1	72.5 ± 1	/
0.025	62.5 ± 1	62.5 ± 1	/
0.05	50.0 ± 1	50.0 ± 1	11.0
0.075	43.0 ± 1	43.0 ± 1	11.5
0.10	/	/	11.9
0.15	/	/	12.7
0.20	/	/	13.6

of all the samples exhibit a logarithmic upturn which progressively flattens with increasing x (see Ref. 10 for a more detailed analysis). At $T \sim 77$ K, FeTe shows a steep drop in the resistivity and the behavior becomes quite metallic below $T \sim 70$ K. In samples with up to 7.5% of Se content, the effect of Se substitution results in a broadening and a shifting to lower temperature of the drop. Samples with $x \geq 0.1$ do not show any feature related to this drop but a flattening of the resistivity followed by an upturn just before the superconducting transition. The superconductive critical temperatures (T_c) increase with Se substitution (Table I), from 11.0 K for the x=0.05 sample up to 13.6 K for the x=0.2 sample.

B. Specific heat

Figure 2 shows the temperature dependence of the heat capacity $C(T)$ of FeTe and FeTe$_{0.975}$Se$_{0.025}$. Slow cooling and heating rates were used and data collected for each thermal cycle. The absolute value of $C(T)$ is very similar for both samples as expected for the minor difference introduced by the very low Se substitution. At high temperatures the absolute value of $C(T)$ tends to saturate at the value of $6R$ predicted by the Dulong-Petit law. Anomalies are clearly visible around 70 and 58 K for FeTe and FeTe$_{0.975}$Se$_{0.025}$, respectively. Consistent with first-order character of this transition thermal hysteresis is present at these transitions (inset of Fig. 2) as already reported by Li *et al.*[7]
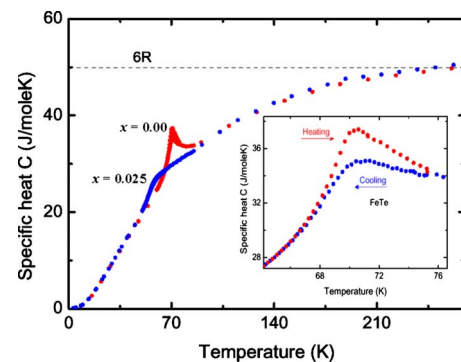

FIG. 2. (Color online) Temperature dependence of the heat capacity $C(T)$ of FeTe and FeTe$_{0.975}$Se$_{0.025}$ samples; the inset shows the thermal hysteresis around transition for FeTe.
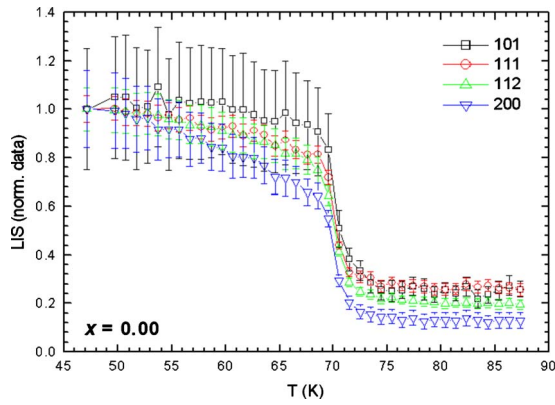
FIG. 3. (Color online) Evolution of the LIS with temperature (normalized data) for the 101,111, 112, and 200 peaks of the FeTe sample.

C. Neutron powder diffraction

In order to investigate whether the structural transition from $P4/nmm$ to $P2/_1m$ occurs in FeTe in one step or if it proceeds via an intermediate $Cmme$ phase, the evolution of the 101, 111, 112, and 200 nuclear peaks was analyzed as a function of temperature using the thermodiffractograms collected on D1B. In fact, all these peaks see a splitting during a tetragonal to monoclinic phase transition, whereas the presence of an intermediate orthorhombic phase would be seen through the splitting of solely the 111 and 112 peaks. In order to verify whether peak splitting occurs at different temperatures, the temperature dependence of the Lorentzian isotropic strain (LIS) contribution to the four aforementioned diffraction peaks was analyzed carrying out a peak fit procedure using an instrumental resolution file of the used diffractometer. This is the most sensitive way of searching for a possible peak broadening caused by an underlying line splitting in cases where the resolution of the diffractometer is not sufficient to detect the splitting directly. Figure 3 shows as an example the evolution of the LIS of the four Bragg peaks with temperature (normalized data) as measured for the FeTe sample. A similar behavior of the same Bragg peaks as a function of temperature was found for all the other measured samples with $x \leq 0.075$, thereby ruling out the occurrence of an intermediate orthorhombic phase. The temperature at which the antiferromagnetic ordering takes place (T_N) is revealed by the arising of magnetic peaks in the NPD patterns. Figure 4 (upper panel) shows the evolution of the NPD pattern of FeTe in the regions of the $\frac{1}{2}$ 0 $\frac{1}{2}$ magnetic peak and the tetragonal 200 nuclear peak, evidencing the simultaneous occurrence of magnetic ordering (T_N) and structural transition (T_{T-M}) at about 70 K. A closer analysis of the evolution of the $\frac{1}{2}$ 0 $\frac{1}{2}$ magnetic peak intensity and of the LIS of the 200 nuclear peak in this temperature region (Fig. 4, lower panel) confirms that both transitions take place simultaneously. T_{T-M} and T_N decrease with increasing Se content but both transitions remain coupled and coincident. The width of the structural and the magnetic transitions increases with substitution (Fig. 5) which can be related to an increasing phase coexistence due to incomplete transition into the monoclinic phase (see below). The important result of this

analysis of the temperature dependence of the magnetic and nuclear Bragg peaks is that $T_{T-M} \cong T_N$ whatever the Se content (critical transition temperatures are reported in Table I). This has to be compared to the situation found in other substituted Fe-based superconductors: in $BaFe_2As_2$, belonging to the so-called 122 family of Fe-based superconductors, the first-order tetragonal to orthorhombic structural transition and the AFM ordering take place simultaneously; Co substitution leads here to a decrease in both transition temperatures but as well to their separation as the magnetic ordering temperature is more rapidly reduced.[11] In the 1111 family Co substitution induces a more complicated behavior: in CaFeAsF, where the structural transition takes place at higher T than the magnetic, 5% of Co doping lowers both transition temperatures which become almost coincident.[12,13] Conversely in $La(Fe_{1-x}Co_x)AsO$ the structural transition is more stable against substitution, whereas magnetism gets rapidly suppressed.[14] If substitution takes place at the rare-earth (RE) site, such as in $(La_{1-y}Y_y)FeAsO$, both transition temperatures are similarly affected by substitution.[15]

Figure 6 (on the left) shows the comparison of the NPD patterns of the four samples in the regions of the $\frac{1}{2}$ 0 $\frac{1}{2}$ magnetic peak and of the tetragonal 200 nuclear peak: a progressive decrease in the magnetic scattering as well as of the peak splitting is observed with the increase in Se substitution. Structural data obtained by Rietveld refinement of the high-resolution NPD data (D1A diffractometer) collected at 2 and 300 K are reported in Tables II–IV; Fig. 7 shows the Rietveld refinement of the NPD data of FeTe collected at 2 K, Fig. 8 shows the evolution of the cell parameters as a function of T below 300 K for the five measured compounds. The substitution of Te by the smaller Se leads to a steady decrease in the cell volume, whereby this effect is mostly caused by the reduction in the cell parameter c; this behavior is related to the fact that the bond length between the tetrahedral Fe and the chalcogen element (Ch=Te,Se) strongly reduces as the Se content increases, whereas the in-plane Fe-Fe bond lengths is almost unaffected (Table II). The occupancies of the Fe sites were refined while the Wyckoff site $2a$ is always fully occupied, slightly different occupancies are obtained at the interstitial site $2c$. This leads to the refined stoichiometries of $Fe_{1+y}Te_{1-x}Se_x$ with $y=0.05,0.04,0.03,0.02,0.02$ for $x=0.00,0.05,0.10,0.15,0.20$, respectively. It becomes evident that the occupation at the site $2c$ (interstitial Fe) decreases with Se substitution. The tetrahedral layer in $Fe_{1+y}Te_{1-x}Se_x$ is much less compressed than the homologous FeAs one in REFeAsO compounds; in fact considering the cube inscribing the tetrahedron centered by Fe, in both cases it results compressed along the c_C axis but in the former case the c_C/a_C ratio is ∼0.9 whereas in the latter one is ∼0.7 (structural data in this case are those reported in Ref. 16 for SmFeAsO; c_C and a_C refers to the edge of the pseudocube, not to be confused with the cell parameters).

Small amounts of a secondary phase (∼5%) are present in all the samples: in particular, for $x=0.00$ the secondary phase is constituted of orthorhombic $FeTe_2$, whereas for the other samples the hexagonal $Fe_{0.67}Te$ phase is present. At 2 K the samples with $x=0.00$ and 0.05 crystallize in the $P2_1/m$ space group (Table III); note that the monoclinic structural model
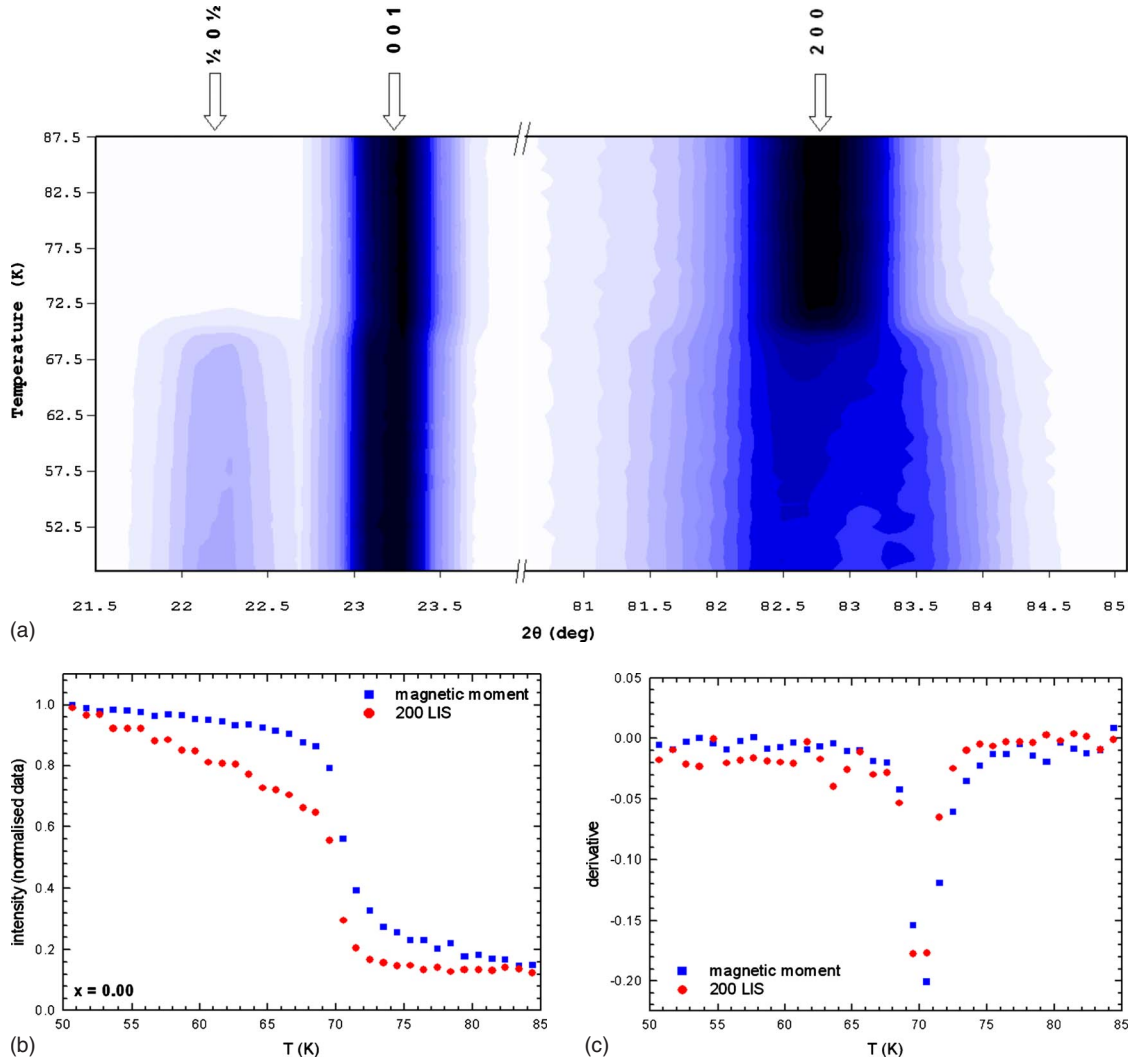
FIG. 4. (Color online) Higher panel: thermodiffractogram of FeTe in the region of the $\frac{1}{2}$ 0 $\frac{1}{2}$ magnetic peak (plus 001 nuclear peak) and the tetragonal 200 nuclear peak, evidencing that magnetic ordering and structural transition occur at the same temperature (D1B data); lower panel: evolution of the $\frac{1}{2}$ 0 $\frac{1}{2}$ magnetic peak intensity and 200 nuclear peak LIS around the structural transition temperature (on the left) and their derivatives (on the right).

of Table III slightly differs from the one previously reported for FeTe by Li *et al.*[7] that located Fe(1) at a 2*b* site with coordinates $\frac{3}{4},\frac{1}{4},z$ and Te as well as Fe(2) at a 2*a* site with coordinates $\frac{1}{4},\frac{1}{4},z$. This structural model is quite debatable: in fact in the $P2_1/m$ space group the coordinates of the 2*a* and 2*b* sites are 0,0,0 and $\frac{1}{2}$,0,0, respectively,[17] and the two
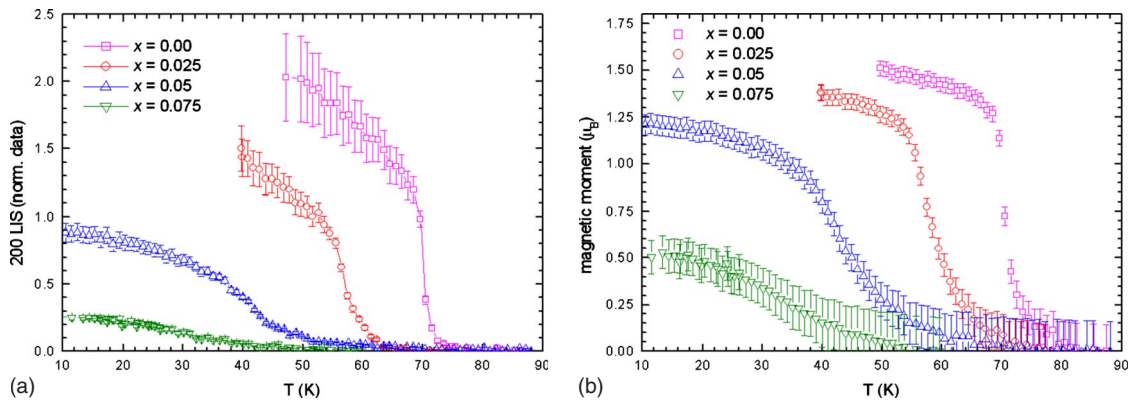

FIG. 5. (Color online) Evolution with temperature of the 200 peak LIS (on the left) and of the magnetic moment (on the right) for samples with $x \leq 0.075$.
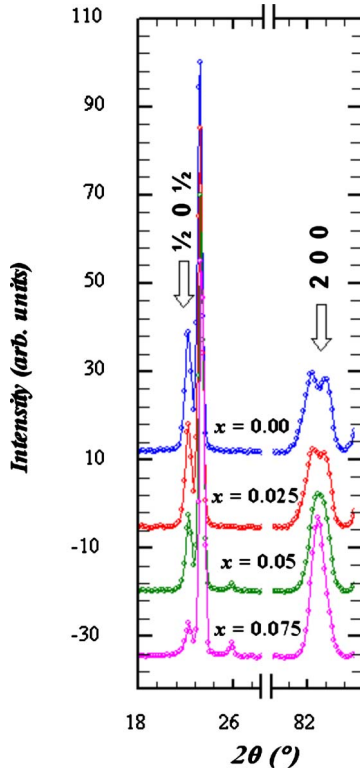
FIG. 6. (Color online) Comparison of the NPD patterns (D1B data) of the samples with $x \leq 0.075$ collected at 2 K on D1B in the regions of the $\frac{1}{2}$ 0 $\frac{1}{2}$ magnetic peak and the tetragonal 200 nuclear peak.
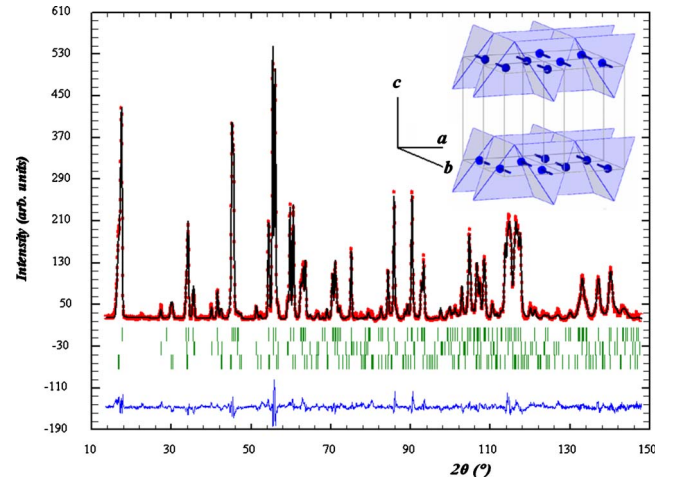

FIG. 7. (Color online) Rietveld refinement plot for FeTe (D1A data collected at 2 K). The points in the upper field represent the observed intensity data, the calculated pattern is superposed and drawn as a solid line; the small vertical bars indicate the position of the allowed Bragg reflections for the FeTe monoclinic nuclear phase (upper), the nuclear orthorhombic $FeTe_2$ phase (intermediate), and the Fe magnetic sublattice (lower); the difference between the observed and calculated patterns is plotted in the lower field. The inset shows the corresponding magnetic structure.

sites are characterized by different site symmetries; conversely in our structural model all atoms are located at the $2e$ site and hence all sites share the same symmetry.

Using the high-resolution data it is possible to ascertain the coexistence of the two polymorphic modifications around $T_{\text{T-M}}$; in fact at 70 K, slight below $T_{\text{T-M}}$, FeTe is, e.g., constituted of ~70% of monoclinic phase, the remaining being tetragonal, whereas in the compound with 5% of Se the amount of monoclinic phase is only ~10% at $T_{\text{T-M}} = 50$ K.

The occurrence of phase coexistence is a clear indication that the tetragonal to monoclinic structural transition is of the first order, as emphasized by specific-heat measurements.

Both samples with $x = 0.00$ and 0.05 exhibit an AFM spin ordering at Fe sublattice characterized by a commensurate magnetic wave vector $\mathbf{q} = (\frac{1}{2} \ 0 \ \frac{1}{2})$ and spins ordered along the b axis (inset of Fig. 7). No component along the x and/or z axis can be detected, differently from what has been observed for $Fe_{1.068}Te$;[7] the magnetic-moment value decreases slightly with Se substitution from $2.54(2)\mu_B$ to $2.08(2)\mu_B$. It is interesting to observe that our $Fe_{1.05}Te$ sample is characterized by the highest value of ordered magnetic moment among those reported in literature.[5,7] A comparison with these data indicates that the value of the magnetic moment of

TABLE II. Structural data for $Fe_{1+y}Te_{1-x}Se_x$ samples obtained by Rietveld refinement of NPD data collected at 300 K ($P4/nmm$ space group; y is the occupancy at Fe(2); bond lengths and angles refer to tetrahedral Fe).

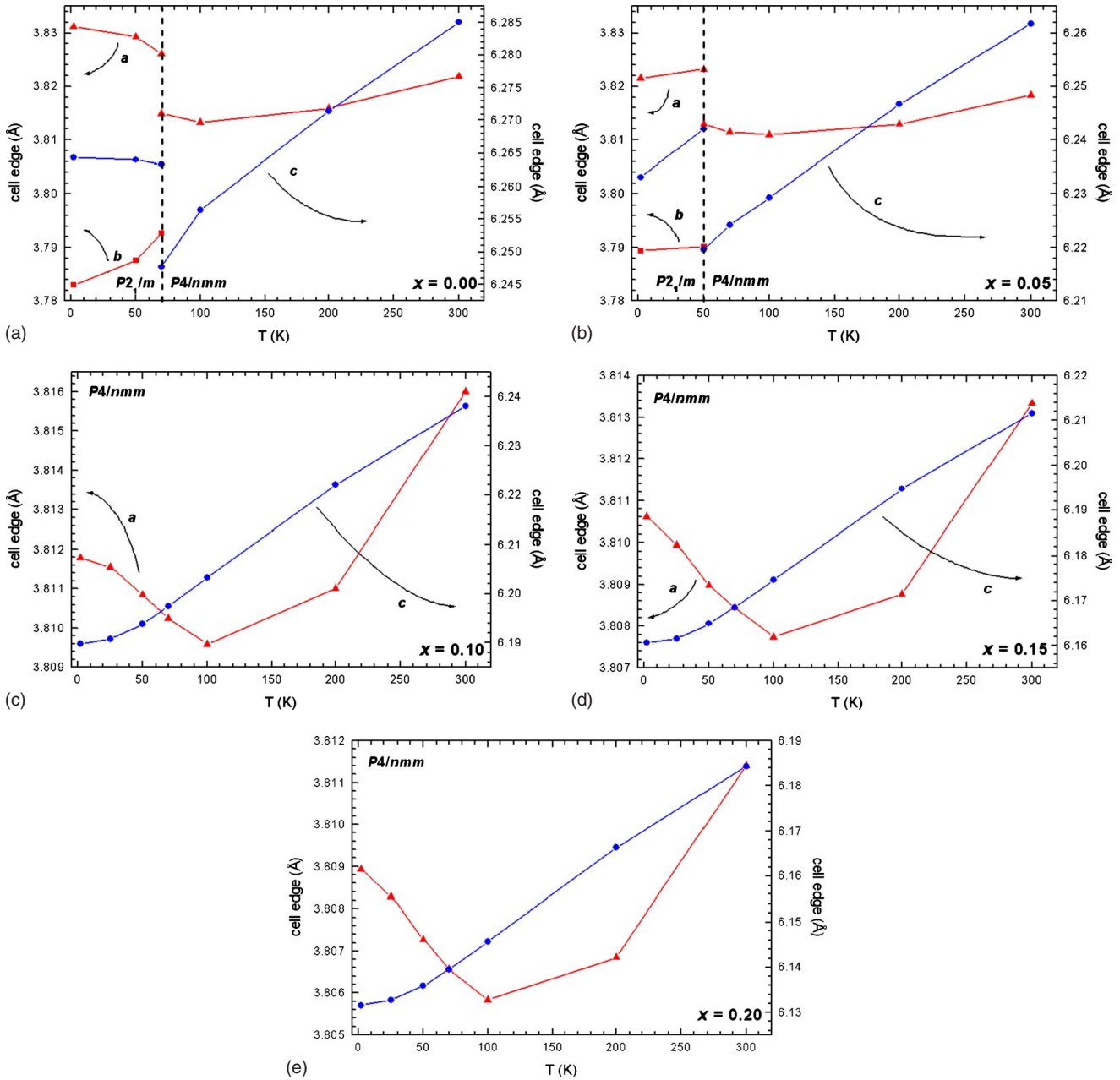|	$x=0.00$	$x=0.05$	$x=0.10$	$x=0.15$	$x=0.20$
a(Å)	3.8219(1)	3.8184(1)	3.8160(1)	3.8133(1)	3.8114(1)
c(Å)	6.2851(1)	6.2617(1)	6.2381(1)	6.2116(1)	6.1843(1)
Fe(1)-$2a$	$\frac{3}{4} \ \frac{1}{4} \ 0$	$\frac{3}{4} \ \frac{1}{4} \ 0$	$\frac{3}{4} \ \frac{1}{4} \ 0$	$\frac{3}{4} \ \frac{1}{4} \ 0$	$\frac{3}{4} \ \frac{1}{4} \ 0$
Fe(2)-$2c$	$\frac{1}{4} \ \frac{1}{4} \ 0.710(4)$	$\frac{1}{4} \ \frac{1}{4} \ 0.718(6)$	$\frac{1}{4} \ \frac{1}{4} \ 0.720(8)$	$\frac{1}{4} \ \frac{1}{4} \ 0.69(1)$	$\frac{1}{4} \ \frac{1}{4} \ 0.675(9)$
y	0.05	0.04	0.03	0.02	0.02
Ch-$2c$	$\frac{1}{4} \ \frac{1}{4} \ 0.2792(4)$	$\frac{1}{4} \ \frac{1}{4} \ 0.2763(4)$	$\frac{1}{4} \ \frac{1}{4} \ 0.2746(4)$	$\frac{1}{4} \ \frac{1}{4} \ 0.2729(4)$	$\frac{1}{4} \ \frac{1}{4} \ 0.2714(4)$
Fe-Ch bond length (Å)	$2.594(2) \times 4$	$2.576(2) \times 4$	$2.564(2) \times 4$	$2.551(2) \times 4$	$2.539(2) \times 4$
Fe-Fe bond length (Å)	$2.702(1) \times 4$	$2.700(1) \times 4$	$2.698(1) \times 4$	$2.696(1) \times 4$	$2.695(1) \times 4$
Ch-Fe-Ch bond angle (deg)	$94.88(5) \times 2$	$95.63(5) \times 2$	$96.17(5) \times 2$	$96.72(5) \times 2$	$97.26(5) \times 2$
	$117.2(1) \times 4$	$116.8(1) \times 4$	$116.5(1) \times 4$	$116.2(1) \times 4$	$115.9(1) \times 4$
R_F (%)	3.52	3.19	2.98	3.17	3.48
R_B (%)	4.47	4.13	4.15	4.27	4.48

FIG. 8. (Color online) Evolution of the cell parameters as a function of T below 300 K.

Fe at the $2a$ site might be correlated with the Fe occupation at the $2c$ site with a higher magnetic moment on $2a$ for lower occupancies on $2c$.

The tetragonal to monoclinic phase transition determines the branching of the Fe-Fe bond distances, as evidenced in Fig. 9 for FeTe. In the monoclinic field the arrangement of the Fe-Fe bonds gives rise to a stripelike pattern oriented along the y axis, different from that observed at low temperature in orthorhombic REFeAsO (Fig. 10). Probably the different spin orderings of the Fe sublattices taking place in FeTe and REFeAsO can be ascribed to the different arrangements of the Fe-Fe bond lengths occurring at low temperature that determine different magnetic exchange paths.

Samples with $x = 0.10, 0.15, 0.20$ retain the tetragonal $P4/nmm$ structure in the whole inspected range, no evidence

for a selective peak broadening can be detected (structural data at 2 K in Table IV) and the magnetic scattering is completely suppressed. In a previous NPD investigation[18] on $Fe_{1+y}Te_{1-x}Se_x$ compounds a pronounced increase in the full width at half maximum of the 200 diffracting peak was observed below 150 K for samples with $0.125 \leq x \leq 0.50$; this behavior was related to a decrease in the lattice symmetry. The microstructural analysis by means of the Williamson-Hall method (see below) of our samples with $0.10 \leq x \leq 0.20$ indicates that not only the $h00$ peaks broaden on cooling but a similar behavior characterizes, e.g., also the $hh0$, the hhh peaks, and in general all those peaks with a strong component lying in the ab plane. This kind of peak broadening must be therefore related to structural strains taking place on cooling in the ab plane, rather than to a structural

TABLE III. Structural data for $Fe_{1+y}Te_{1-x}Se_x$ samples obtained by Rietveld refinement of NPD data collected at 2 K ($P2_1/m$ space group; bond lengths and angles refer to tetrahedral Fe).

	$x=0.00$	$x=0.05$
a(Å)	3.8312(1)	3.8216(1)
b(Å)	3.7830(1)	3.7893(1)
c(Å)	6.2643(1)	6.2331(1)
β (deg)	89.17	89.37
Fe(1)-2e	0.7616(1) $\frac{1}{4}$ 0.0035(4)	0.7591(1) $\frac{1}{4}$ 0.0030(4)
Fe(2)-2e	0.229(1) $\frac{1}{4}$ 0.714(1)	0.246(1) $\frac{1}{4}$ 0.683(1)
Ch-2e	0.2580(1) $\frac{1}{4}$ 0.2800(1)	0.2571(1) $\frac{1}{4}$ 0.2751(1)
Fe-Ch bond length (Å)	2.5740(3)$\times$2	2.5463(3)$\times$2
	2.5962(2)$\times$2	2.5630(3)$\times$2
Fe-Fe bond length (Å)	2.7568(2)$\times$2	2.7411(2)$\times$2
	2.6295(2)$\times$2	2.6420(2)$\times$2
Ch-Fe-Ch bond angle (deg)	93.53(1)$\times$1	95.02(1)$\times$1
	95.76(2)$\times$1	96.83(2)$\times$1
	115.56(1)$\times$2	115.20(1)$\times$2
	119.08(1)$\times$2	118.03(1)$\times$2
$\mu(\mu_B)$	2.54(2)	2.08(2)
R_F (%)	3.52	2.70
R_B (%)	4.47	3.68

transition. This structural strains probably originates the faint negative thermal expansion along the a axis observed below 100 K (Fig. 8), a phenomenon observed in previous NPD investigations[18] and in thermal-expansion measurements carried out on $FeTe_{0.5}Se_{0.5}$ single crystal.[19]

The evolution of the cell volume as a function of T can be described by

$$V(T) = \gamma\chi_S \cdot U(T) + V(0), \qquad (1)$$

where χ_S is the adiabatic compressibility, γ the Grüneisen parameter, $U(T)$ the internal energy, and $V(0)$ the volume at the lowest temperature. From D1B-NPD data, the experimental dependence of the cell volume as a function of T between 2 and 80 K is available only for the $x=0.05$ and 0.075 samples. As evaluated by integrating specific-heat data, the samples with $x=0.00$ and 0.025 are characterized by the same value of $U(T)$ (inset of Fig. 11); hence we can confidently assume that also the sample with $x=0.05$ is characterized by a similar value of $U(T)$. For this reason the value of $U(T)$ estimated by specific heat was introduced in Eq. (1) to describe $V(T)$ of the sample with 5% of Se and compare the result with experimental data (Fig. 11). A good agreement is obtained below $T_{\text{T-M}} \cong T_N(\sim 50$ K) for $\gamma\chi_S \sim 2.1 \times 10^{-10}$ Pa^{-1}, a value similar to that reported for single crystal $Fe_{1.06}Te$ in the monoclinic phase region.[19] Above $T_{\text{T-M}}$, in the tetragonal phase region, the experimental data depart from those estimated by Eq. (1). Around $T_{\text{T-M}}$ this behavior can be due to the presence of latent heat that is not properly accounted in bare heat-capacity data; however with increasing T the reduced thermal expansion takes place. Such a behavior, observed also for $Fe_{1.06}Te$ (see Fig. 5 in Ref. 19), suggests that in the AFM phase also the magnetic excitation
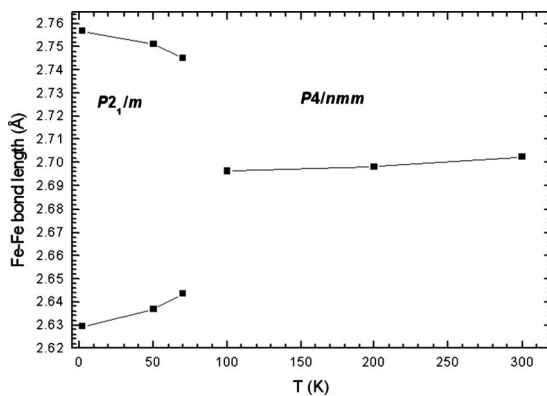

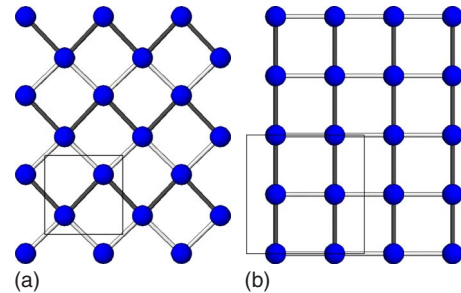FIG. 9. Evolution of the Fe-Fe bond lengths as a function of T in FeTe.

FIG. 10. (Color online) Stripelike pattern originated by Fe-Fe bonds in monoclinic FeTe (on the left) compared to the pattern occurring in orthorhombic REFeAsO (on the right; shorter bonds: empty sticks and longer bonds: full sticks).

TABLE IV. Structural data for $Fe_{1+y}Te_{1-x}Se_x$ samples obtained by Rietveld refinement of NPD data collected at 2 K ($P4/nmm$ space group; bond lengths and angles refer to tetrahedral Fe).

	$x=0.10$	$x=0.15$	$x=0.20$
a(Å)	3.8118(1)	3.8106(1)	3.8089(1)
c(Å)	6.1898(1)	6.1606(1)	6.1316(1)
Fe(1)-2a	$\frac{3}{4}$ $\frac{1}{4}$ 0	$\frac{3}{4}$ $\frac{1}{4}$ 0	$\frac{3}{4}$ $\frac{1}{4}$ 0
Fe(2)-2c	$\frac{1}{4}$ $\frac{1}{4}$ 0.695(6)	$\frac{1}{4}$ $\frac{1}{4}$ 0.690(7)	$\frac{1}{4}$ $\frac{1}{4}$ 0.707(7)
Ch-2c	$\frac{1}{4}$ $\frac{1}{4}$ 0.2738(3)	$\frac{1}{4}$ $\frac{1}{4}$ 0.2719(3)	$\frac{1}{4}$ $\frac{1}{4}$ 0.2713(3)
Fe-Ch bond length (Å)	2.5504(1)×4	2.5369(1)×4	2.5287(1)×4
Fe-Fe bond length (Å)	2.6953(1)×4	2.6945(1)×4	2.6933(1)×4
Ch-Fe-Ch bond angle (deg)	96.71(4)×2	97.36(4)×2	97.73(4)×2
	116.20(9)×4	115.85(9)×4	115.64(9)×4
R_F (%)	2.22	2.53	3.01
R_B (%)	3.28	3.55	3.65

contributes as well to the Grüneisen parameter, whereas this contribution disappears above $T_{T-M} \cong T_N$.

Information on the effect of the Se substitution on the microstructure of the samples was obtained analyzing the broadening of NPD lines (high resolution—D1A data) by means of the Williamson-Hall plot method.[20] Generally, in the case where size effects are negligible and the strain is isotropic, a straight line passing through all the points and through the origin has to be observed, where the slope provides the lattice strain: the higher the slope, the higher the strain. If the broadening is not isotropic, size and strain effects along some crystallographic directions can be obtained by considering different orders of the same reflection. In our case, for each sample, the size contribution is negligible since a straight line passing through the origin can be traced. Figure 12 shows the superposition of the Williamson-Hall plots obtained by the microstructural analysis of the data collected at 300 K on D1A; for clarity only selected diffraction peaks are reported and indexed. It is evident that in pure

FeTe microstrain is almost isotropic since a straight line can be traced passing approximately through all the diffracting peaks. The Se substitution induces strain along the [001] direction, increasing with increasing Se content, whereas the strain in the ab plane is almost unaffected by the degree of substitution. The compression of the tetrahedral layer, measured as the c_C/a_C ratio of the pseudocube inscribing the FeCh$_4$ tetrahedron, increases with the increase in the Se content and this is reflected in the changes experienced by the Ch-Fe(1)-Ch bond angles. Two kinds of Ch-Fe(1)-Ch bond angles are present, the former bisected by the c axis, widening with the substitution, the latter that conversely contracts with the increase in the Se content (Table II). The increase in T_c observed in samples with $x \gtrsim 0.05$ is probably related to these structural and microstructural features. This is in agreement with the findings of Bud'ko *et al.*[19] which argued that in-plane pressure should decrease T_c, whereas a pressure along c should lead to an increase. Interestingly, in thin films, the behavior seems to be exactly the opposite, as T_c increases with the decrease in cell parameter a, that is, with the increase in the compressive strain in the Fe plane.[21] Note that in these thin films the value of the cell parameter a is
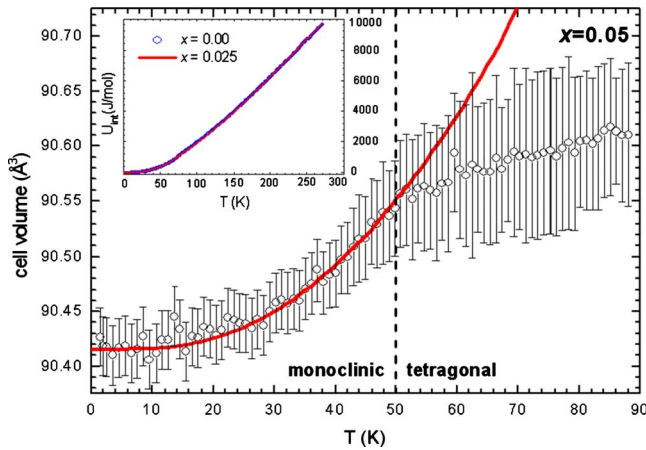

FIG. 11. (Color online) Evolution of the cell volume for $x=0.05$ below 90 K (D1B data) fitted with Eq. (1) (solid curve); the inset shows the internal energy of the samples with $x=0.00$ and 0.025 between 0 and 270 K, as evaluated by integrating specific-heat data.
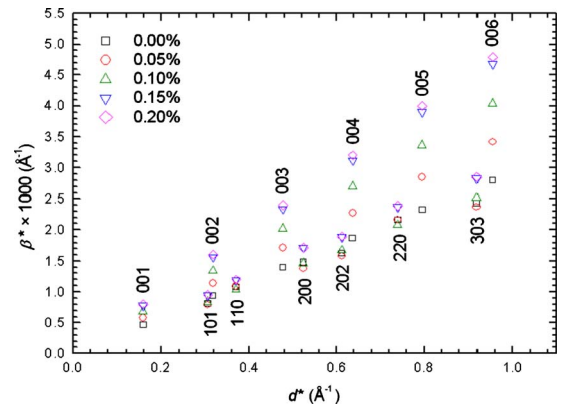

FIG. 12. (Color online) Superposition of the Williamson-Hall plots obtained by the microstructural analysis of the data collected at 300 K on D1A; only selected diffraction peaks are reported and indexed.

strongly dependent on both the nature of the substrate and the film thickness but results in any case shorter than the one measured on the bulk sample.

In this context it is interesting to observe that density-functional calculations foresee a transition from the observed double stripe AFM spin ordering and $(\pi, 0)$ spin fluctuations to a single stripe one and (π, π) spin fluctuations as the distance of Ch from the Fe plane (half edge of the pseudocube along c) decreases below ~ 1.72 Å.[22] In particular, it has been suggested that superconductivity in Fe chalcogenides may be related to (π, π) spin ordering and fluctuations. As can be easily calculated from the data reported in Table II, in the sample bearing 5% of Se, characterized by $T_N \sim 50.0 \pm 1$ K and $T_c = 11.0$ K, the distance of Ch from the Fe plane is ~ 1.73 Å and in the sample with 10% this distance decreases to ~ 1.71 Å, LR-AFM ordering is suppressed and only superconductivity takes place ($T_c = 11.9$ K). This result is thus in very good agreement with density-functional calculations foreseeing superconductivity when (π, π) spin ordering and fluctuation become dominant.[22] In any case it must be underlined that several neutron magnetic scattering experiments[5–8] ascertained that even in the SR-AFM regime, appearing for Se contents exceeding the critical value of about 10 at. %, an incommensurate wave vector $\mathbf{q} = (\frac{1}{2} - \delta \; 0 \; \frac{1}{2})$ is present, similar to one occurring in the LR-AFM regime; this result suggests that the type of spin fluctuation does not change with Se content. Theoretical calculations suggest that the structural transition is partly determined by orbital ordering, involving a cooperative Jahn-Teller distortion, rather than spin ordering; as a result double exchange interactions can take place leading to the observed AFM structure.[23]

In this context it is worth to note that: (1) SR-AFM incommensurate order[5–8] has been observed in samples with x up to ~ 0.45, inside which the magnetic volume fractions is strongly dominant (generally exceeding 90%),[8] but characterized by a tetragonal structure at low T;[5,7] (2) in both SR and LR-AFM regimes the magnetic wave vector is the same, except for its slight incommensurability in the SR-AFM regime; (3) for pure FeTe the T_N obtained by NPD analysis (sensitive only to LR-AFM interactions) and by muon-spin rotation[8] (sensitive also to SR-AFM interactions) is the same, thus suggesting that SR-AFM interactions are absent above the structural transition; (4) the magnetic transition temperatures reported in literature[8] for SR-AFM ordering are in good agreement with those that we obtained for LR-AFM ordering by analyzing the neutron thermodiffractograms, as plotted in Fig. 13. These facts suggest that LR-AFM order can take place only when the structural transition is not suppressed by Se substitution in FeTe. Above a critical value of Se content, located in the range $0.075 \leq x \leq 0.10$, the structural transition is suppressed and only SR magnetic interactions can take place, their percolation into a LR-AFM structure being hindered. Conversely the occurrence of the monoclinic structure favors magnetic interactions, as shown in Fig. 13 where the samples undergoing this structural transition are character-
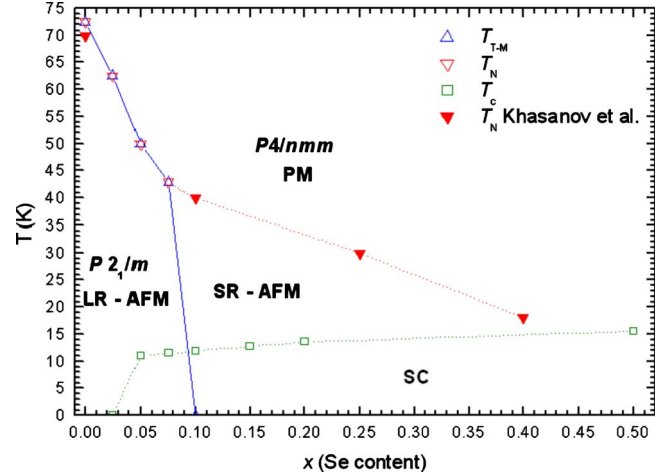

FIG. 13. (Color online) Phase diagram of the system FeTe$_{1-x}$Se$_x$ for $x \leq 0.50$ showing the stability field of the LR-AFM interactions as obtained from our NPD data (empty symbols) compared with the field of the SR-AFM interactions reported by Khasanov *et al.* (Ref. 8) (full symbols); note that the tetragonal to monoclinic phase transition is first order and hence, strictly speaking, the stability fields of the two polymorphs should be separated by a two-phase region.

ized by a steep rise of T_N. This conclusion is also supported by the fact that magnetism is not the driving force for the tetragonal to orthorhombic phase transition taking place at 90 K in the tetragonal isostructural and superconducting Fe$_{1.01}$Se compound.[4] In any case further investigations are needed in order to exactly ascertain the role of magnetic interactions in the tetragonal to orthorhombic structural transition of FeTe.

IV. CONCLUSIONS

Samples with nominal composition Fe$_{1+y}$Te$_{1-x}$Se$_x$ ($0 \leq x \leq 0.20$) were analyzed by neutron powder diffraction between 2 and 300 K. Rietveld refinement indicates that samples with $x \leq 0.075$ undergo a first-order tetragonal to monoclinic phase transition, whose temperature decreases with increasing Se content. This structural transition is accompanied by a simultaneous antiferromagnetic ordering at the tetrahedral Fe site. Differently from what has been observed in other families of Fe-based superconductors, the structural and the long-range magnetic transitions in Fe$_{1+y}$Te$_{1-x}$Se$_x$ remain coincident after Se substitution. In samples with $x \geq 0.10$ the structural phase transition as well as the long-range magnetic ordering are suppressed. Superconductivity is observed for $x \geq 0.05$, although zero resistivity occurs only for $x \geq 0.10$. Se substitution produces a cell compression, a decrease in the Ch height over the Fe plane and an increase in the Ch-Fe-Ch tetrahedral bond angle. It is likely that the structural transition is not driven by magnetic interactions but conversely that long-range magnetic order can take place only if the structural transition is not suppressed by Se substitution in FeTe.

*Corresponding author; amartin@chimica.unige.it

[1] Y. Kamihara, T. Watanabe, M. Hirano, and H. Hosono, J. Am. Chem. Soc. **130**, 3296 (2008).

[2] H. Okamoto and L. E. Tanner, in *Binary Alloy Phase Diagrams*, edited by T. B. Massalski (ASM International, Cleveland, OH, 1990), Vol. 2, p. 1781.

[3] H. Okamoto, in *Binary Alloy Phase Diagrams*, edited by T. B. Massalski (ASM International, Cleveland, OH, 1990), Vol. 2, p. 1769.

[4] T. M. McQueen, A. J. Williams, P. W. Stephens, J. Tao, Y. Zhu, V. Ksenofontov, F. Casper, C. Felser, and R. J. Cava, Phys. Rev. Lett. **103**, 057002 (2009).

[5] W. Bao, Y. Qiu, Q. Huang, M. A. Green, P. Zajdel, M. R. Fitzsimmons, M. Zhernenkov, S. Chang, M. Fang, B. Qian, E. K. Vehstedt, J. Yang, H. M. Pham, L. Spinu, and Z. Q. Mao, Phys. Rev. Lett. **102**, 247001 (2009).

[6] J. Wen, G. Xu, Z. Xu, Z. W. Lin, Q. Li, W. Ratcliff, G. Gu, and J. M. Tranquada, Phys. Rev. B **80**, 104506 (2009).

[7] S. Li, C. de la Cruz, Q. Huang, Y. Chen, J. W. Lynn, J. Hu, Y.-L. Huang, F.-C. Hsu, K.-W. Yeh, M.-K. Wu, and P. Dai, Phys. Rev. B **79**, 054503 (2009).

[8] R. Khasanov, M. Bendele, A. Amato, P. Babkevich, A. T. Boothroyd, A. Cervellino, K. Conder, S. N. Gvasaliya, H. Keller, H.-H. Klauss, H. Luetkens, V. Pomjakushin, E. Pomjakushina, and B. Roessli, Phys. Rev. B **80**, 140511(R) (2009).

[9] J. Rodríguez-Carvajal, Physica B **192**, 55 (1993).

[10] M. Tropeano, I. Pallecchi, M. Cimberle, C. Ferdeghini, G. Lamura, M. Vignolo, A. Martinelli, A. Palenzona, and M. Putti, arXiv:0912.0395 (unpublished).

[11] D. K. Pratt, W. Tian, A. Kreyssig, J. L. Zarestky, S. Nandi, N. Ni, S. L. Bud'ko, P. C. Canfield, A. I. Goldman, and R. J. McQueeney, Phys. Rev. Lett. **103**, 087001 (2009).

[12] S. Takeshita, R. Kadono, M. Hiraishi, M. Miyazaki, A. Koda, S. Matsuishi, and H. Hosono, Phys. Rev. Lett. **103**, 027002 (2009).

[13] Y. Xiao, Y. Su, R. Mittal, T. Chatterji, T. Hansen, C. M. N. Kumar, S. Matsuishi, H. Hosono, and Th. Brueckel, Phys. Rev. B **79**, 060504(R) (2009).

[14] C. Wang, Y. K. Li, Z. W. Zhu, S. Jiang, X. Lin, Y. K. Luo, S. Chi, L. J. Li, Z. Ren, M. He, H. Chen, Y. T. Wang, Q. Tao, G. H. Cao, and Z. A. Xu, Phys. Rev. B **79**, 054521 (2009).

[15] A. Martinelli, A. Palenzona, M. Tropeano, C. Ferdeghini, M. R. Cimberle, and C. Ritter, Phys. Rev. B **80**, 214106 (2009).

[16] A. Martinelli, M. Ferretti, P. Manfrinetti, A. Palenzona, M. Tropeano, M. R. Cimberle, C. Ferdeghini, R. Valle, C. Bernini, M. Putti, and A. S. Siri, Supercond. Sci. Technol. **21**, 095017 (2008).

[17] *International Tables for Crystallography*, 5th ed., edited by T. Hahn (Springer, New York, 2005), Vol. A.

[18] K. Horigane, H. Hiraka, and K. Ohoyama, J. Phys. Soc. Jpn. **78**, 074718 (2009).

[19] S. L. Bud'ko, P. C. Canfield, A. S. Sefat, B. C. Sales, M. A. McGuire, and D. Mandrus, Phys. Rev. B **80**, 134523 (2009).

[20] J. I. Langford, D. Louër, E. J. Sonneveld, and J. W. Visser, Powder Diffr. **1**, 211 (1986).

[21] E. Bellingeri, I. Pallecchi, R. Buzio, A. Gerbi, D. Marrè, M. R. Cimberle, M. Tropeano, M. Putti, A. Palenzona, and C. Ferdeghini, Appl. Phys. Lett. **96**, 102512 (2010).

[22] C. Moon and H. Choi, Phys. Rev. Lett. **104**, 057003 (2010).

[23] A. M. Turner, F. Wang, and A. Vishwanath, Phys. Rev. B **80**, 224504 (2009).